

Quantum Criticality in the infinite-range Transverse Field Ising Model

Nicholas Curro, Kaeshav Danesh and Rajiv R. P. Singh
University of California Davis, CA 95616, USA
(Dated: August 7, 2024)

We study quantum criticality in the infinite range Transverse-Field Ising Model. We find subtle differences with respect to the well-known single-site mean-field theory, especially in terms of gap, entanglement and quantum criticality. The calculations are based on numerical diagonalization of Hamiltonians with up to a few thousand spins. This is made possible by the enhanced symmetries of the model, which divide the Hamiltonian into many block-diagonal sectors. The finite temperature phase diagram and the characteristic jump in heat capacity closely resemble the behavior in mean-field theory. However, unlike mean-field theory where excitations are always gapped, the excitation gap in the infinite range model goes to zero from both the paramagnetic side and from the ferromagnetic side on approach to the quantum critical point. Also, contrary to mean-field theory, at the quantum critical point the Quantum Fisher Information becomes large, implying long-range multi-partite entanglement. We find that the main role of temperature is to shift statistical weights from one conserved sector to another. However, low energy excitations in each sector arise only near the quantum critical point implying that low energy quantum fluctuations can arise only in the vicinity of the quantum critical field where they can persist up to temperatures of order the exchange constant.

INTRODUCTION

Recent studies of quadrupolar transverse-field Ising behavior in thulium vanadate materials have raised important questions about quantum criticality in such systems [1–3]. The finite temperature thermodynamic behavior shows a jump in the heat-capacity characteristic of mean-field behavior that is expected for phonon-mediated systems with long-range interactions [1, 4]. Yet, surprisingly, NMR spin-echo experiments show a dramatic wipe-out phenomena extending over a fan-like region in the temperature-transverse field plane near the quantum critical field, signifying persistent quantum critical fluctuations [5]. The well known single-site mean-field theory captures the phase diagram and the jump in the heat capacity quite well. However, the mean-field theory always has a large energy gap and hence no low energy fluctuations that can cause rapid decoherence of NMR signals [6]. The purpose of this work is to study a concrete model that has mean-field thermodynamic behavior and yet may support persistent quantum critical fluctuations.

We consider a system of N half integer spins. The infinite range Transverse-Field Ising Model (TFIM) Hamiltonian can be expressed in terms of Pauli spin matrices for the i th spin σ_i^α as

$$\mathcal{H} = -\frac{J}{2N} \left(\sum_i \sigma_i^z \right)^2 - h_x \sum_i \sigma_i^x. \quad (1)$$

We will set $J = 1$, which sets all energy scales.

MEAN-FIELD THEORY

The standard mean-field theory replaces the Hamiltonian by a single site effective Hamiltonian [7, 8]

$$\mathcal{H}_{eff} = -m_z \sigma^z - h_x \sigma^x, \quad (2)$$

where the magnetization m_z needs to be determined self-consistently

$$m_z = \langle \sigma^z \rangle. \quad (3)$$

Various physical properties are easy to calculate in this approximation. It leads to a transition temperature as a function of transverse-field given by

$$T_c(h_x) = h_x / \tanh^{-1}(h_x). \quad (4)$$

In our units the zero field transition temperature $T_c(0)$ and the critical field at zero temperature h_c are both unity.

The mean-field approximation is known to be exact in the thermodynamic limit for the classical model ($h_x = 0$). In this study we explore deviations from the mean-field behavior for the infinite-range model for non-zero h_x and the implications for quantum critical phenomena. We note that the infinite range model has been derived as a zeroth order model for the thulium vanadate and other quadrupolar transverse-field Ising materials where gapless phonons mediate long-range interactions between the Ising degrees of freedom [1, 4, 9, 10].

INFINITE-RANGE MODEL

The infinite range model has a large number of symmetries. Because the Hamiltonian depends only on two

operators

$$S_z = \sum_i S_i^z, \quad (5)$$

and

$$S_x = \sum_i S_i^x, \quad (6)$$

both of which commute with the total spin operator

$$S_t^2 = \sum_i S_i^2, \quad (7)$$

the Hamiltonian becomes block diagonal into many relatively small ($O(N)$) Hilbert-space sectors [11, 12]. The energy levels and properties in each sector depend on the total spin s_t , which can take values from 0 to $N/2$ (we will assume N is even). The spin sector has Hilbert space dimension $2s_t + 1$. The number of copies of the spin s_t sector is the number of ways N spin-half objects can be combined into total spin s_t . This number $d(s_t)$ is one for $s_t = N/2$ and for $s_t < N/2$ can be expressed in terms of the combinatoric factors C_n^m as

$$d(s_t) = C_{N/2+s_t}^N - C_{N/2+s_t+1}^N. \quad (8)$$

In each s_t sector the Hamiltonian matrix can be written out in terms of the matrix elements of spin operators and diagonalized numerically. Thus, given the symmetries it is possible to numerically calculate energy eigenlevels of the system with up to a few thousand spins rather than few tens of spins for most lattice models.

Energy gap

The ground state always lies in the largest s_t sector. Energy gap between the lowest excited states and the ground state are shown in Fig. 1 and Fig. 2 as a function of the transverse-field h_x . In the $N \rightarrow \infty$ limit, there are two degenerate ground states in the ordered phase at $h_x < 1$. One can see the difference between the energies of the first two states in Fig. 1. With increasing system size this is rapidly going to zero for $h < h_c$. To measure the excitation energy below h_c one needs to look at the next excited state in the ordered phase. This excitation energy is shown in Fig. 2.

From the two figures, a key difference from the single site mean-field theory becomes clear. In mean-field theory the gap does not go below $2J$. It goes to zero at h_c in the infinite-range model as expected at the quantum critical point. The gap vanishes as one approaches the quantum critical point h_c from either side. Furthermore, at the quantum critical point, one expects a whole cascade of states to come down to zero energy in the thermodynamic limit.

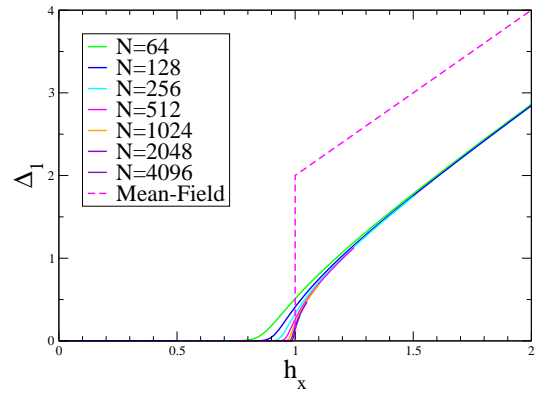


FIG. 1. Energy difference between the lowest two states. Note that for $h < h_c = 1$, there are two degenerate states in the thermodynamic limit and hence this energy difference goes to zero. Mean-field theory results are shown by dashed lines.

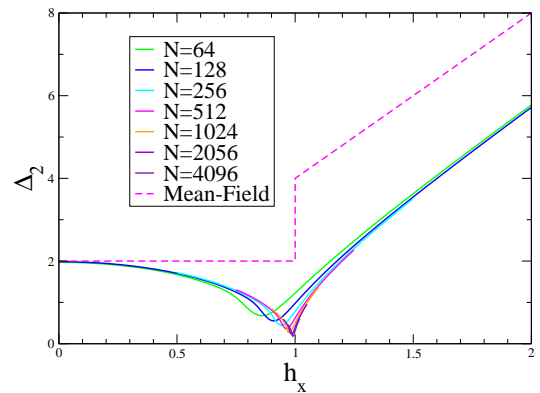


FIG. 2. Energy difference between the third lowest energy state and the ground state showing that excitation energy goes to zero from both sides as one approaches the quantum critical point. Mean-field theory results are shown by dashed lines.

To see how the gap vanishes with system size N at the quantum critical point, we show a log-log plot of several energy gaps as a function of system size in Fig. 3. All the states shown exhibit gaps vanishing as $N^{-1/3}$ as $N \rightarrow \infty$ (See also Ref. [13]).

The two lowest excitations in the paramagnetic phase, within a sector, can be identified with one and two spin-flip excitations. Even for large h_x the gap stays below the mean-field value by an amount $J = 1$ and $2J = 2$ within a given s_t sector. As shown in the Appendix, this result can be obtained from perturbation theory around the large field limit and shows that deviations from mean-field theory are present for all fields and not just near the critical field.

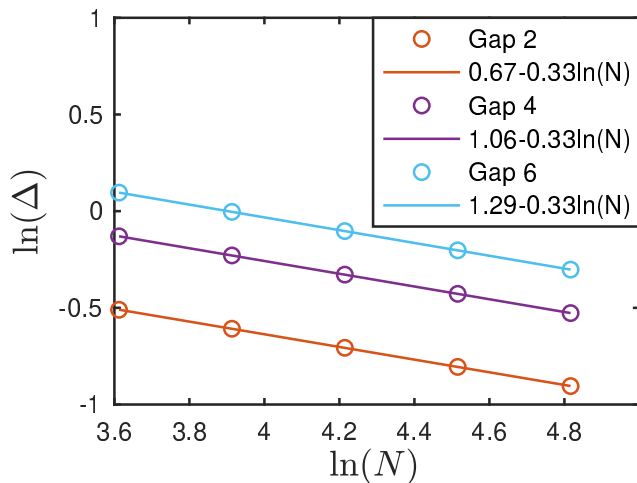


FIG. 3. Log-log plot of energy gaps vs N at the quantum critical point for several low lying states showing the gap scaling as $N^{-1/3}$.

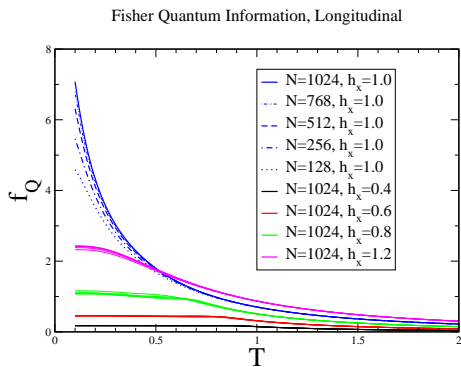


FIG. 4. A plot of the Quantum Fisher Information further confirms the quantum critical nature by showing the build up of quantum entanglement in the thermodynamic state at low temperatures near the quantum critical point.

Quantum Fisher Information

In mean field theory, the quantum state factorizes and does not have any quantum entanglement between different sites, even at the quantum critical point. One can consider multi-particle entanglement as one of the defining properties of quantum criticality. To look for multi-partite entanglement in the infinite-range model, we turn to Quantum Fisher Information QFI [11]. QFI is the generalization of Fisher Information from classical statistics to a quantum mechanical system. For a pure state, the QFI associated with a variable \hat{O} is simply proportional to its variance. In a mixed state, such as at finite temperatures, let the i th eigenstate of the system have probability p_i . Then the QFI F_Q for the observable

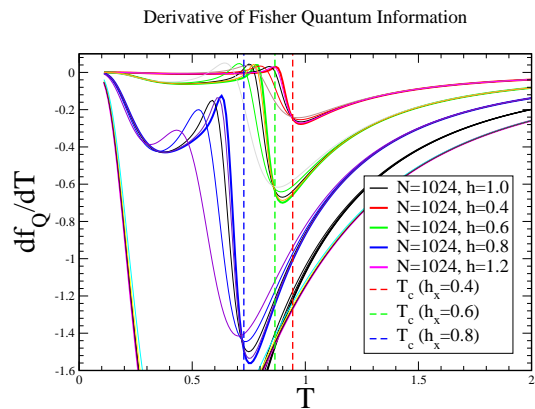


FIG. 5. Derivative of the Quantum Fisher Information with respect to temperature shows that f_Q inherits the energy singularity and hence its derivative has a discontinuity like the heat capacity at the finite temperature transition. Note that the thinner lines correspond to the same parameter as the solid line but for smaller system sizes ($N = 768, 512$ and 256) to indicate how the curves move with size of the system.

\hat{O} is given by the expression [11]:

$$F_Q = 2 \sum_{i,j} \frac{(p_i - p_j)^2}{p_i + p_j} | \langle i | \hat{O} | j \rangle |^2. \quad (9)$$

The QFI is a witness of multi-particle entanglement. For a system of N spin-half objects, if the QFI per site for any extensive variable \hat{O} defined as

$$f_Q = F_Q/N, \quad (10)$$

exceeds some integer m (for sufficiently large N), then there is at least $m + 1$ -particle entanglement in the system.

The operator with the largest Quantum Fisher Information for our model is:

$$\hat{O} = S_z, \quad (11)$$

where S_z is the total z-component of the spin-operator defined in Eq. 5. All QFI calculations will be shown for this operator. Figure 4 shows f_Q for several system sizes. Note that for a proper calculation at finite temperatures one must sum over all states of the system and not just consider one spin sector of the Hilbert space [11]. It is clear that near the quantum critical point at low temperatures f_Q becomes large and this means that the system becomes highly entangled. Note also that the Quantum Fisher Information decreases more rapidly at $T = 0$ in the ordered phase than in the disordered phase. This is consistent with the behavior of other measures of quantum entanglement such as Renyi entanglement entropy (See e.g. Ref. [14]).

Figure 5 shows the derivative of f_Q with respect to temperature for different transverse field values. One

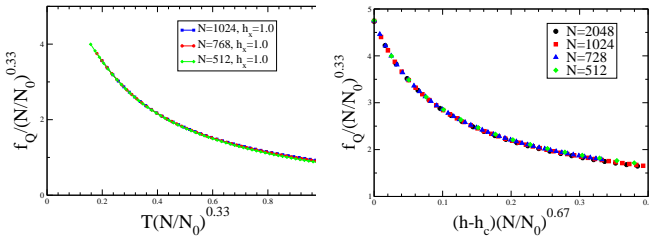


FIG. 6. Scaling plots of Quantum Fisher Information f_Q at critical field h_c versus T (left) and at $T = 0$ versus transverse-field (right) for different system sizes N . We have scaled N by a fixed reference size $N_0 = 128$.

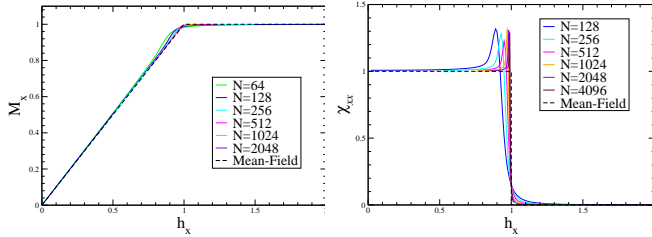


FIG. 7. Plot of the transverse magnetization M_x (left) and transverse susceptibility χ_{xx} (right) as a function of the transverse field in the ground state of the system. Mean-field results are shown by dashed lines.

finds a characteristic behavior of a sharp maxima followed by a minima, which presumably becomes a discontinuity in the thermodynamic limit. This feature tracks the critical temperatures at different fields which are shown by dashed lines. This is not surprising as measures of quantum entanglement can inherit an energy-like singularity even at a finite temperature phase transition, just from the singular changes in the density of states at the finite temperature critical point [15–17]. Note however that this finite temperature singularity does not mean there is any enhanced multi-particle quantum entanglement at the classical phase transition, as the magnitude of f_Q remains small away from the quantum critical region.

Quantum Critical Properties of the Quantum Fisher Information

At $T = 0$, QFI reduces to the variance of the operator S_z in the ground state of the system, up to an overall factor. Near the quantum critical point $N \rightarrow \infty$, $T \rightarrow 0$, $h \rightarrow h_c$, homogeneity [18] implies, we can write the singular piece of QFI as

$$f_Q(N, T, h) = N^a X(T N^b, (h - h_c) N^c), \quad (12)$$

where $X(x, y)$ is a scaling function of two variables. Fig. 6 shows the scaling plots for (a) $h = h_c$ and (b) $T = 0$ with

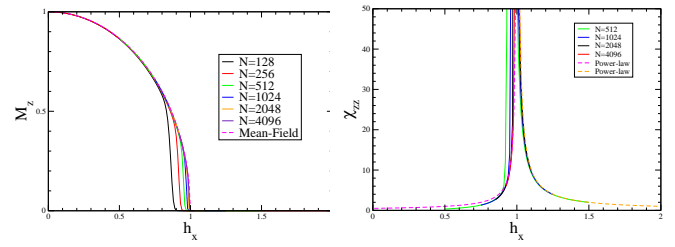


FIG. 8. A plot of the longitudinal magnetization (left) and longitudinal susceptibility (right) as a function of the transverse-field in the ground state of the system obtained with a small symmetry-breaking field $h_z = 0.0001$.

exponents $a = 1/3$, $b = 1/3$, $c = 2/3$. Note that the exponent b is consistent with the expected T/Δ scaling with the gap Δ vanishing with power $N^{-1/3}$.

Our scaling relations imply that in the thermodynamic limit, at $h = h_c$, f_Q diverges as $1/T$ as $T \rightarrow 0$ and furthermore, at $T = 0$, f_Q diverges as $(h - h_c)^{-1/2}$. The latter exponent is consistent with the expected divergence in the mean-field universality class with a critical exponent $\gamma - z\nu = 1/2$, with $\gamma = 1$, $z = 1$ and $\nu = 1/2$.

Ground-state magnetization and susceptibilities

The transverse magnetization M_x and susceptibility χ_{xx} in the ground state can be obtained by taking derivatives of the ground state energy with h_x . To calculate the longitudinal magnetization or order parameter M_z and the order parameter susceptibility χ_{zz} one needs to add a small symmetry-breaking field. These quantities are shown in Figs. 7 and 8. Deviations from mean-field theory is most pronounced in the transverse susceptibility near the quantum critical point $h_x = h_c$. In the mean-field theory the transverse susceptibility is a constant below h_c and the magnetization M_x increases linearly with the field. In the infinite range model there is very little deviation from mean-field results in the thermodynamic limit ($N \rightarrow \infty$) away from the critical point. However, an enhanced susceptibility very near the critical point with a sharp peak at the transition seems to persist with increasing N as seen in Fig. 7. Note that the jump in the transverse susceptibility reflects the mean-field critical behavior and is not special to the infinite-range model. Singularities in longitudinal magnetization and susceptibility are consistent with mean-field critical exponents as shown by fits to mean-field behavior in Fig 8. That is, $M_z \simeq |h_x - h_c|^\beta$ and $\chi_{zz} \simeq |h_x - h_c|^{-\gamma}$ with $\beta = 1/2$ and $\gamma = 1$.

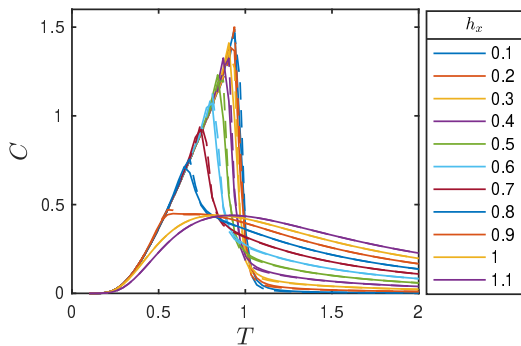


FIG. 9. Heat capacity as a function of temperature for various values of the transverse field for $N = 1024$ spins. The solid lines are for $N = 1024$ and the dashed lines for $N = 2048$.

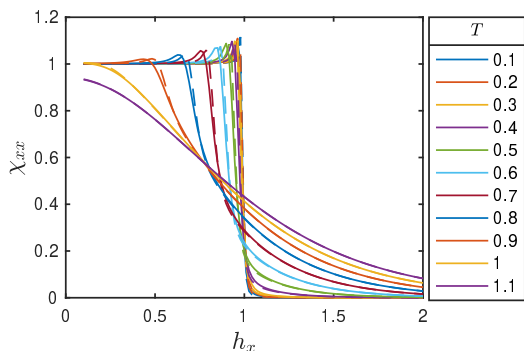


FIG. 10. Transverse susceptibility as a function of transverse-field for fields for various temperatures for the infinite-range model. Solid lines are for $N = 1024$ and dashed lines for $N = 2048$.

FINITE TEMPERATURE THERMODYNAMIC PROPERTIES AND THULIUM VANADATES

Thermodynamic properties such as entropy, heat capacity and transverse susceptibilities at finite temperatures can be obtained from the partition function of the system. The partition function is given by:

$$\begin{aligned} Z(T, h_x) &= \text{Tr} \exp(-\beta \mathcal{H}) \\ &= \sum_{s_t} d(s_t) \sum_{i \in s_t} e^{-\beta E_i}, \end{aligned} \quad (13)$$

where $d(s_t)$ is the number of sectors with spin s_t in the system.

A plot of the calculated heat capacity as a function of temperature is shown in Fig. 9 for a range of transverse-field values. The system studied is large enough to exhibit the characteristic jump like feature of mean-field theory as observed in the TmVO₄ materials [1].

Transverse-susceptibility as a function of field for various temperatures is shown in Figure 10, and as a function

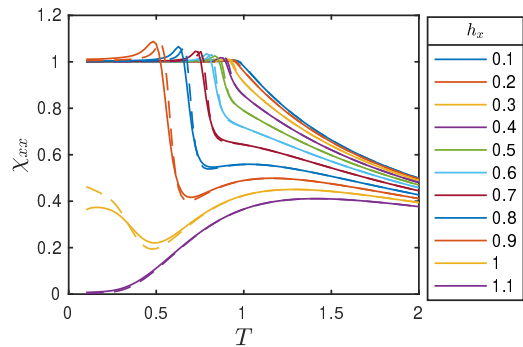


FIG. 11. Transverse susceptibility as a function of temperature for various transverse fields for the infinite-range model. Solid lines are for $N = 1024$ and dashed lines for $N = 2048$.

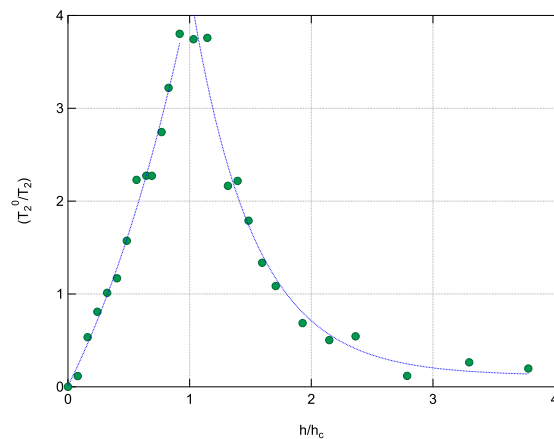


FIG. 12. Normalized spin decoherence rate, $T_2^0/T_2 = -\log(I(h)/I(0))$ measured in TmVO₄ at $T = 0.77$ [5]. Here I is the integrated spectral intensity measured by spin echoes, normalized such that $I(0)$ is unity, and the constant $T_2^0 \approx 6 \times 10^{-5}$ sec. The sharp rise at the quantum critical field is indicative of quantum criticality.

of temperature for various fields in Figure 11. In mean-field theory the susceptibility is constant in the ordered phase and jumps at the transition as a function of field and then rapidly decreases in the paramagnetic phase. The most visible difference from mean-field theory is the rise of the transverse susceptibility in the ordered phase above the mean-field value and a small but distinct peak near the quantum critical point. At low temperatures, this peak increases with increase in temperature. Such a peak may be observable in the materials.

The TmVO₄ materials

Our study provides a resolution of the different behaviors observed in the thermodynamic and NMR spin-echo measurements in the thulium vanadate materials.

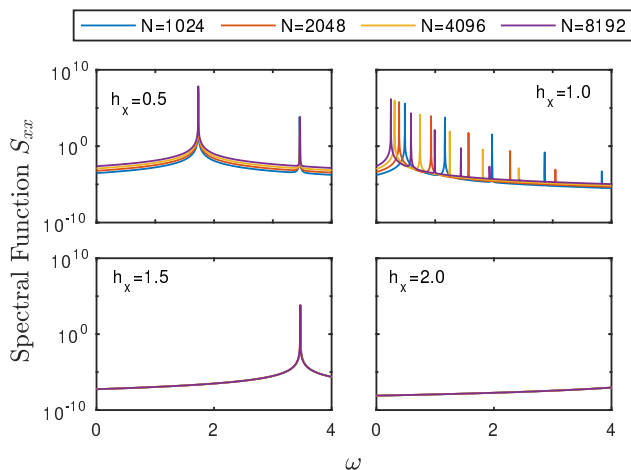


FIG. 13. Spectral weights associated with the total transverse spin with delta functions broadened by a Lorentzian of width $\eta = 10^{-5}$ for transverse-field values of 0.5, 1.0, 1.5 and 2.0. Away from the quantum critical point at $h_x = h_c = 1$, the system has a large gap. At the quantum critical point, a number of states converge towards zero energy with increase in system size.

The phase diagram and heat capacity jump of the model closely follow mean-field theory. These are well reproduced by the infinite-range model. However, unlike mean-field theory, NMR spin-echo measurements show persistent low energy quantum critical fluctuations near the critical field. As an example, the divergent spin-spin relaxation rate is shown in Fig. 12. The infinite range transverse-field Ising model shows that both the mean-field thermodynamic and low energy spectral behaviors can be simultaneously present in a long-ranged system.

In Fig. 13, we show the spectral function associated with the total transverse spin operator. In these finite systems, the spectral weights consist of a series of delta-function peaks that have been broadened by a Lorentzian with a broadening parameter $\eta = 10^{-5}$. The spectral functions are shown on a logarithmic scale. One can see that away from the quantum critical point at $h_c = 1$, there is a gap in the spectra of order J which is almost size independent. This gap is too large to cause any low frequency NMR relaxation. In contrast, at the critical point $h_c = 1$ a whole series of states are converging towards zero energy. It is these states at low energies, characteristic of a quantum critical point, that can cause a rapid decoherence of the nuclear spins.

The main effect of temperature in the model is that the probability of finding the system in a spin-sector s_t changes as a function of temperature. Probability distribution for finding the system in different spin-sectors, for two different values of the transverse-field, for a system of $N = 1024$ spins are shown in Fig. 14 for temperatures up to twice the zero-field transition temperature. At low

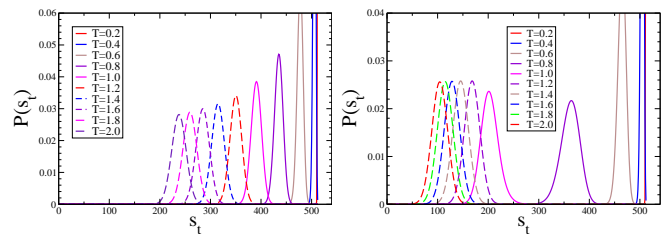


FIG. 14. Probability distribution for finding the system in spin-sector S at the critical field $h_c = 1$ (left) and deep inside the ordered phase $h_c = 0.4$ (right) at several temperatures for a system of $N = 1024$ spins with maximum spin of $s_t = 516$. For $h < h_c$, such as $h_c = 0.4$, there is a finite temperature phase transition and the largest shift in the probability distribution happens as one crosses the phase transition.

temperatures (up to about $T = 0.2$) this probability is very sharply peaked near the highest spin sector, where the ground state resides. Even at twice the ordering temperature the probability is still peaked in a spin sector that is a fraction of the maximum spin, hence extensive in number of spins. It would take an unphysically large temperature for the probability to finally shift to sectors with spin of order one. One can also see in the plot that the largest change in the probability distribution occurs as one crosses the phase transition.

In each such sector with an extensive spin value, the system supports low energy quantum dynamics near the critical field. That is, the gaps go to zero in every large spin sector at h_c . As the main role of temperature is to shift the probability distribution to reduced s_t values, low energy weight remain at the critical field even as temperature increases. This tells us that for a sufficiently large system the quantum critical fluctuations can persist at the quantum critical point to temperatures of order the exchange constant. We note that it has been shown in literature that in a one-dimensional transverse-field Ising model, quantum critical fluctuations persist up to infinite temperature [6, 19].

SUMMARY

In summary, we have shown that the infinite range transverse-field Ising model exhibits quantum criticality. The energy gap goes to zero as the quantum critical field is approached from either side of the transition. The study of Quantum Fisher Information shows that the system becomes highly entangled as the quantum critical point is approached in the temperature-field plane. While the Quantum Fisher Information appears to be singular at the finite temperature phase transition, it does not serve as a witness for enhanced quantum entanglement along the finite temperature phase boundary away from the quantum critical region. In other words,

the enhanced multi-partite quantum entanglement is observed only in the quantum critical region.

Various thermodynamic quantities show deviations from mean-field behavior especially near the quantum critical field. Heat capacity has a jump at the transition which closely resembles the mean-field behavior. However, the transverse susceptibility shows a peak at $T = 0$ near the quantum critical point, unlike mean-field theory. At finite temperatures also a small but distinct peak in the transverse susceptibility remains. The spectral function associated with the transverse-susceptibility shows low energy weights only near the quantum critical point, which persists over a range of temperatures.

This study points to a possible consistent explanation of the various observed properties in the Thulium Vanadate materials. While the heat capacity in the material shows a jump quite similar to mean-field theory, NMR studies find quantum critical features with a vanishing spin-gap and a rapid decoherence of nuclear spin states in the vicinity of the quantum critical field consistent with the results of our model study. We also find peaks in the transverse susceptibility at low temperatures in the quantum critical region and speculate that such peaks should be present for phonon mediated transverse-field Ising systems that can be modelled with long-range interactions.

We thank I. Fisher and I. Vinograd for stimulating discussions. This Work was supported by the NSF under Grants No. DMR-2210613 and PHY-1852581.

[1] P. Massat, J. Wen, J. M. Jiang, A. T. Hristov, Y. Liu, R. W. Smaha, R. S. Feigelson, Y. S. Lee, R. M. Fernandes, and I. R. Fisher, Field-tuned ferroquadrupolar quantum phase transition in the insulator TmVO₄, *Proc. Natl. Acad. Sci.* **119**, e2119942119 (2022).

[2] I. Vinograd, K. R. Shirer, P. Massat, Z. Wang, T. Kissikov, D. Garcia, M. D. Bachmann, M. Horvatić, I. R. Fisher, and N. J. Curro, Second order Zeeman interaction and ferroquadrupolar order in TmVO₄, *npj Quantum Materials* **7**, 68 (2022).

[3] Z. Wang, I. Vinograd, Z. Mei, P. Menegasso, D. Garcia, P. Massat, I. R. Fisher, and N. J. Curro, Anisotropic nematic fluctuations above the ferroquadrupolar transition in TmVO₄, *Phys. Rev. B* **104**, 205137 (2021).

[4] G. A. Gehring and K. A. Gehring, Co-operative Jahn-Teller effects, *Rep. Prog. Phys.* **38**, 1 (1975).

[5] Y.-H. Nian, I. Vinograd, T. Green, C. Chaffey, P. Massat, R. R. P. Singh, M. P. Zic, I. R. Fisher, and N. J. Curro, Spin-echo and quantum versus classical critical fluctuations in TmVO₄, [arXiv:2306.13244 \[cond-mat.str-el\]](https://arxiv.org/abs/2306.13244) (2023), [arXiv:2306.13244](https://arxiv.org/abs/2306.13244).

[6] S.-W. Chen, Z.-F. Jiang, and R.-B. Liu, Quantum criticality at high temperature revealed by spin echo, *New J. Phys.* **15**, 043032 (2013).

[7] P. G. de Gennes, Collective motions of hydrogen bonds, *Solid State Communications* **1**, 132 (1963).

[8] R. B. Stinchcombe, Thermal and magnetic properties of the transverse Ising model, *Journal of Physics C: Solid State Physics* **6**, 2507 (1973).

[9] U. Karahasanovic and J. Schmalian, Elastic coupling and spin-driven nematicity in iron-based superconductors, *Phys. Rev. B* **93**, 064520 (2016).

[10] I. Paul and M. Garst, Lattice effects on nematic quantum criticality in metals, *Phys. Rev. Lett.* **118**, 227601 (2017).

[11] L. T. Philipp Hauke, Markus Heyl and P. Zoller, Measuring multipartite entanglement through dynamic susceptibilities, *Nature Physics* **12**, 778 (2016).

[12] F. V. Johannes Wilms, Julien Vidal and S. Duduel, Finite temperature mutual information in a simple phase transition, *Journal of Statistical Mechanics: Theory and Experiments* **12**, 1 (2016).

[13] S. Dusuel and J. Vidal, Finite-size scaling exponents of the Lipkin-Meshkov-Glick model, *Phys. Rev. Lett.* **93**, 237204 (2004).

[14] R. R. P. Singh, R. G. Melko, and J. Oitmaa, Thermodynamic singularities in the entanglement entropy at a two-dimensional quantum critical point, *Phys. Rev. B* **86**, 075106 (2012).

[15] T.-C. Lu and T. Grover, Singularity in entanglement negativity across finite-temperature phase transitions, *Phys. Rev. B* **99**, 075157 (2019).

[16] T.-C. Lu and T. Grover, Structure of quantum entanglement at a finite temperature critical point, *Phys. Rev. Res.* **2**, 043345 (2020).

[17] N. E. Sherman, T. Devakul, M. B. Hastings, and R. R. P. Singh, Nonzero-temperature entanglement negativity of quantum spin models: Area law, linked cluster expansions, and sudden death, *Phys. Rev. E* **93**, 022128 (2016).

[18] B. Widom, Equation of state in the neighborhood of the critical point, *J. Chem. Phys.* **43**, 3898 (1965).

[19] H. T. Quan, Z. Song, X. F. Liu, P. Zanardi, and C. P. Sun, Decay of Loschmidt echo enhanced by quantum criticality, *Phys. Rev. Lett.* **96**, 140604 (2006).

APPENDIX

In this appendix we develop high-field perturbation theory for the infinite-range model to show that the gaps in excitation energy have finite corrections to the mean-field results even in the limit that the transverse-field h_x goes to infinity. In mean-field theory, the entire paramagnetic phase is described by decoupled spins in a transverse field, for which the excitation gap corresponding to flipping a spin has energy $2h_x$. We consider the maximum S_t sector of our infinite-range model in which the ground state lies for all h_x . In this sector, all states correspond to a uniform state analogous to a $q = 0$ state in finite dimensional system.

In the ground state for h_x going to infinity, all spins are pointing in the x-direction. Its energy can be calculated perturbatively and gives

$$E_0 = -Nh_x - \frac{J^2}{16h_x}, \quad (14)$$

as $h_x \rightarrow \infty$ corrections to mean-field result goes to zero. The one-particle state or single spin-flip state is an equal superposition of spin-flip states at each site. Its energy already changes in first order perturbation theory due to matrix elements connecting flipped spins at different sites leading to

$$E_1 = -(N - 2)h_x - J. \quad (15)$$

Similarly, the energy of two-spin flip state has energy

$$E_2 = -(N - 4)h_x - 2J. \quad (16)$$

This shows that as h_x goes to infinity, there remains a correction to energy gaps from the mean-field result. The one-particle excitation has a gap of $2h_x - J$ and two-particle gap has excitation gap $4h_x - 2J$.

This figure "Chi-MFT.png" is available in "png" format from:

<http://arxiv.org/ps/2408.02789v1>

This figure "Delta1.png" is available in "png" format from:

<http://arxiv.org/ps/2408.02789v1>

This figure "DeltaE1.png" is available in "png" format from:

<http://arxiv.org/ps/2408.02789v1>

This figure "Delta2.png" is available in "png" format from:

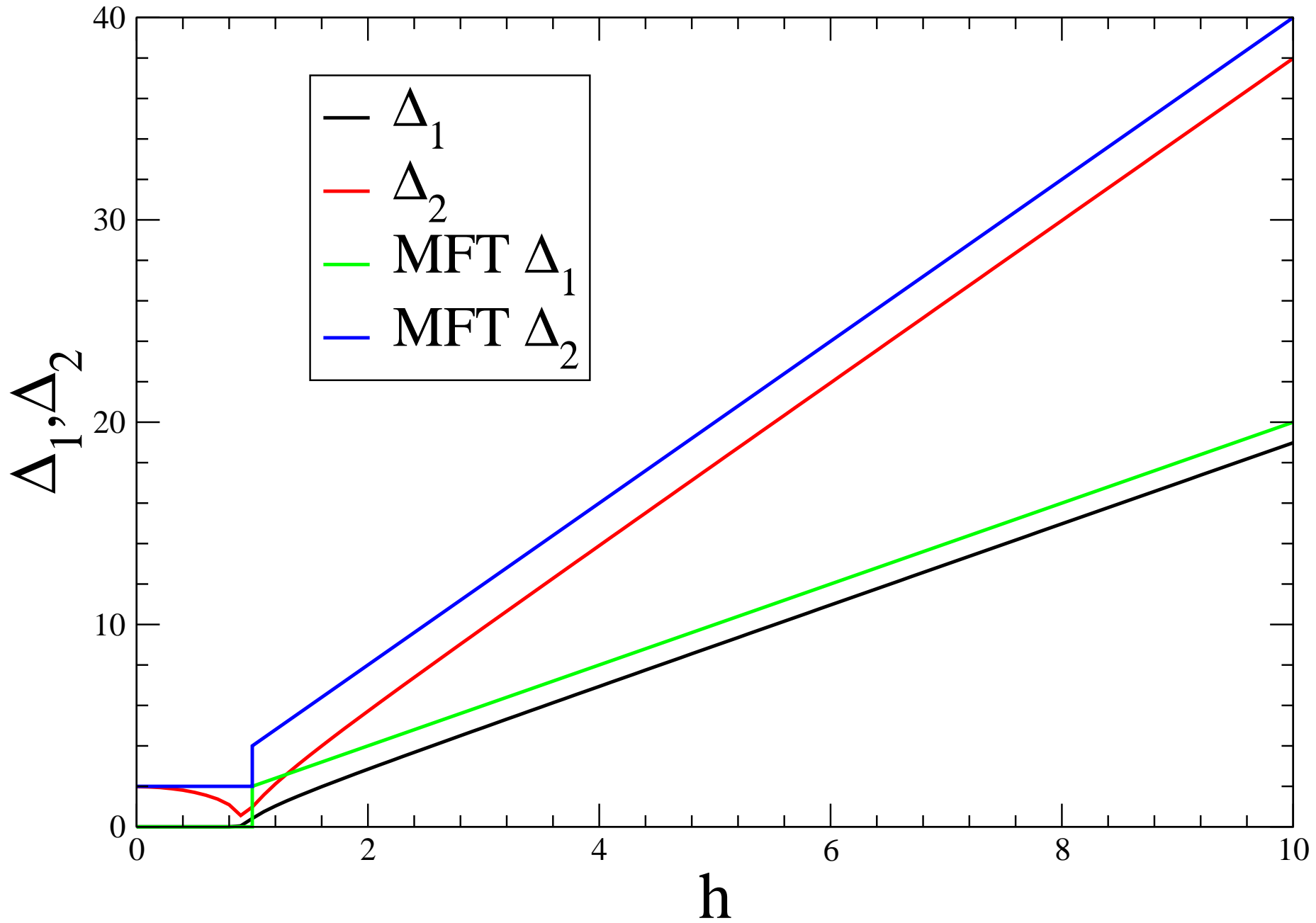
<http://arxiv.org/ps/2408.02789v1>

This figure "DeltaE2.png" is available in "png" format from:

<http://arxiv.org/ps/2408.02789v1>

Solution of mean-field model

N=128



This figure "Large-h.png" is available in "png" format from:

<http://arxiv.org/ps/2408.02789v1>

This figure "N512-chi-T.png" is available in "png" format from:

<http://arxiv.org/ps/2408.02789v1>

This figure "N512-chi.png" is available in "png" format from:

<http://arxiv.org/ps/2408.02789v1>

This figure "N512-cv.png" is available in "png" format from:

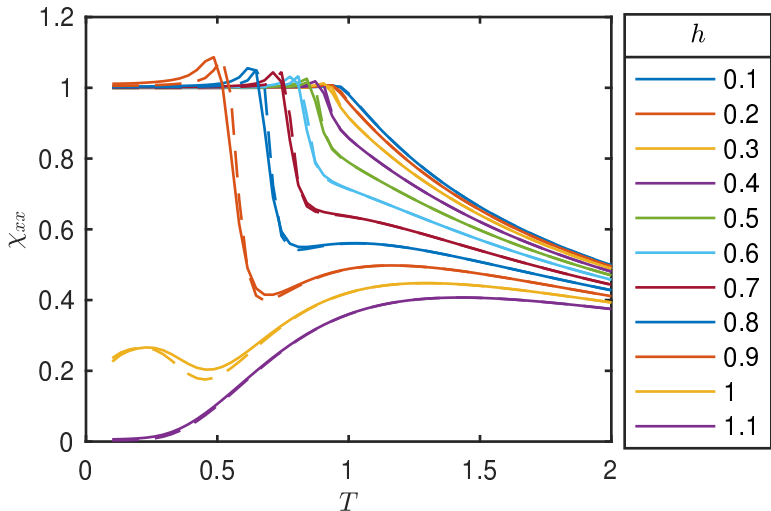
<http://arxiv.org/ps/2408.02789v1>

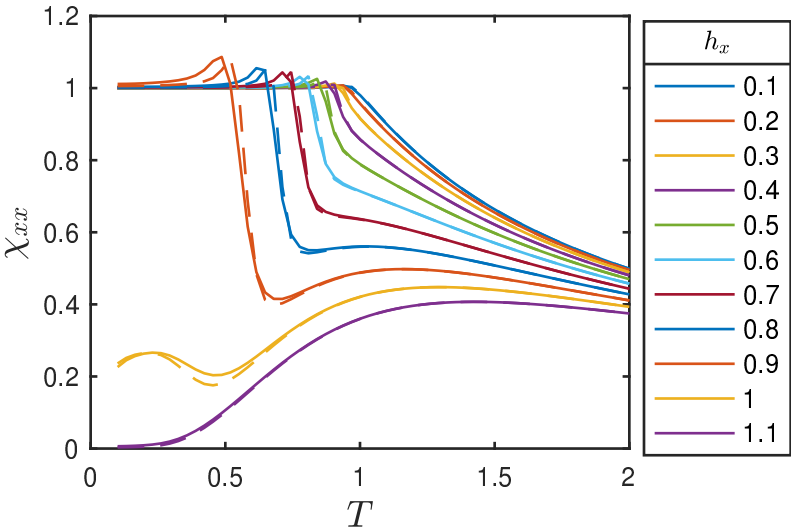
This figure "Spectral-weights.jpg" is available in "jpg" format from:

<http://arxiv.org/ps/2408.02789v1>

This figure "chixx.png" is available in "png" format from:

<http://arxiv.org/ps/2408.02789v1>





This figure "chiz.png" is available in "png" format from:

<http://arxiv.org/ps/2408.02789v1>

This figure "dfqdT.png" is available in "png" format from:

<http://arxiv.org/ps/2408.02789v1>

This figure "mx.png" is available in "png" format from:

<http://arxiv.org/ps/2408.02789v1>

This figure "mz.png" is available in "png" format from:

<http://arxiv.org/ps/2408.02789v1>